Finite elements method and blurry images

José Exequiel Fuentes Gil, Numerical Analysis II Project

Introduction

When you want to capture an image it may not correspond to the desired scene. This may be due to several factors such as what can be:

1. Environmental factors (cloudiness, humidity).
2. Defects of the capture device (lenses, sensors).
3. The scene itself, for example, what you want to capture is in motion.

This phenomenon appears in several situations: when the Hubble telescope was released on April 26, 1990, the first images were blurred images like images shown in Figure 6. When a camera activates portrait mode, it blurs everything except the person to whom the photo is taken, like is shown in Figure 7. The security cameras and speed cameras take photos of objects in motion, like cars and people, these images have a motion blur of the object, like Figure 8. Keeping this in mind, it is important to develop a model for blurred images. For this is necessary to know how the images are treated. A gray-scale image is understood as a scalar function

$$\begin{aligned} Gr : \mathbb{R}^2 &\longrightarrow \mathbb{R} \\ (x, y) &\longrightarrow Gr(x, y) \end{aligned}$$

where $Gr(x, y)$ is the intensity value of the point (x, y) this value is a number between 0 and 255. this scale indicates that 0 is black and 255 is white.

A color image is composed of three "fundamental" colors: red, green and blue, this becomes to the image format whose initials are R, G, and B, known simply as RGB format. This kind of image is understood as a vectorial function

$$\begin{aligned} I : \mathbb{R}^2 &\longrightarrow \mathbb{R}^3 \\ (x, y) &\longrightarrow I(x, y) = (R(x, y), G(x, y), B(x, y)) \end{aligned}$$

where $R(x, y)$, $G(x, y)$ and $B(x, y)$ are red, green and blue colors respectively also called color channels, each of them gray-scale images.

(a) Color image (b) Red channel (c) Green channel (d) Blue channel

Figure 1: Northern Lights image and its color channels. Recovered from [9]

Finally, the dimensions of an image are given by the number of pixels they have, they are mentioned in the same way as the dimensions of a matrix. In the case of the Figure 1 has dimensions 800×534 pixels.

The blurring degradation phenomenon can be modeled by a partial differential equation; more exactly with a heat equation. The image can be seen as a plate with an initial temperature distribution and the degradation effect as the heat diffusion process. In this case, the lens is responsible for blurring the light that comes to it, an assumption is that the lens only distributes the light that comes to it, does not absorb it. From now on, the blurring model will be applied on each color channel separately. In this way it will be assumed that each image is a gray-scale image, alluding to each color.

Model in partial differential equations

By making the analogy with a plate with heat distribution, a model of this type can be used. In this case the objective is to find $u : \Omega \times [0, T] \longrightarrow \mathbb{R}$ such that

$$\begin{aligned} \frac{\partial u}{\partial t} - div(k(x,y)\nabla u) = 0 \\ u(x,y,0) = I(x,y), \ \frac{\partial u}{\partial \eta} = 0 \ in \ \partial\Omega. \end{aligned} \tag{1}$$

Where:

- u is the image degrading over time. That is to say, for each time $\hat{t}$ the image $I_{\hat{t}}(x,y) = u(x,y,\hat{t})$ represents the original image in a certain state of degradation,
- $k(x,y)$ is the diffusion coefficient, it controls the intensity and direction of the degradation,
- $I(x,y)$ it is the original image, without degrading,

- $\dfrac{\partial u}{\partial \eta}$ is the flow at the boundary of Ω, here, it indicates that the sum of the intensity values of the image does not change, according to the lens hypothesis and
- $\Omega \subseteq \mathbb{R}^2$ is the domain of the problem when dealing with images this domain is a rectangle whose extension is given by the dimensions of the image. Each point in the domain represents the intensity value of the image at that point.

Weak Formulation

To give the weak formulation of the differential equation (1) the space $H^1(\Omega)$ is chosen and a test function $v \in H^1(\Omega)$ is used to integrate the first term of (1) as follows

$$\iint_\Omega \frac{\partial u}{\partial t} v \; dA - \iint_\Omega div(k \nabla u) v \; dA = 0,$$

using the first Green's identity

$$\iint_\Omega \frac{\partial u}{\partial t} v \; dA - \iint_\Omega div(kv \nabla u) \; dA + \iint_\Omega k(\nabla u \cdot \nabla v) \; dA = 0,$$

and the divergence's theorem

$$\iint_\Omega \frac{\partial u}{\partial t} v \; dA - \int_{\partial \Omega} k(x) v (\nabla u \cdot \eta) \; ds + \iint_\Omega k(\nabla u \cdot \nabla v) \; dA = 0,$$

the boundary condition implies that $\dfrac{\partial u}{\partial \eta} = \nabla u \cdot \eta = 0$ in $\partial \Omega$, that is

$$\iint_\Omega \frac{\partial u}{\partial t} v \; dA + \iint_\Omega k(\nabla u \cdot \nabla v) \; dA = 0,$$

to add the implicit Euler method, let $t_0, \ldots, t_M$ a partition of $[0, T]$, $u_n = u(x, t_n)$ and $\Delta t_n = t_n - t_{n-1}$ for $n = 1, \ldots, M$. The derivative approximation $\dfrac{\partial u}{\partial t} = \dfrac{u_n - u_{n-1}}{\Delta t_n}$ is used as

$$\iint_\Omega \frac{u_n - u_{n-1}}{\Delta t_n} v \; dA + \iint_\Omega k(\nabla u_n \cdot \nabla v) \; dA = 0,$$

with this, the weak formulation of (1) is obtained: find $u_0, \ldots, u_M \in H^1(\Omega)$ such that

$$\begin{gathered} \iint_\Omega u_n v \; dA + \Delta t_n \iint_\Omega k \nabla u_n \cdot \nabla v \; dA = \iint_\Omega u_{n-1} v \; dA \\ u_0 = I(x, y), \quad \textit{for each } v \in H^1(\Omega) \textit{ and } n = 1, 2, \ldots, M. \end{gathered} \tag{2}$$

To give the Petrov-Garlekin formulation the image domain Ω structure is considered. The nodes in the domain are given by the pixels, in this way the elements are formed by four nodes arranged in a square shape, see Figure 2. In each element S there are four degrees of freedom,

so the use of the bilinear elements space Q_1 for the representation of u and the test functions v is proposed.

$$Q_1 = \{E(x,y) \in H^1(\Omega) : E(x,y)|_S = a + bx + cy + dxy,\ a,b,c,d \in \mathbb{R},\ \textit{for each element } S \subseteq \Omega\}$$

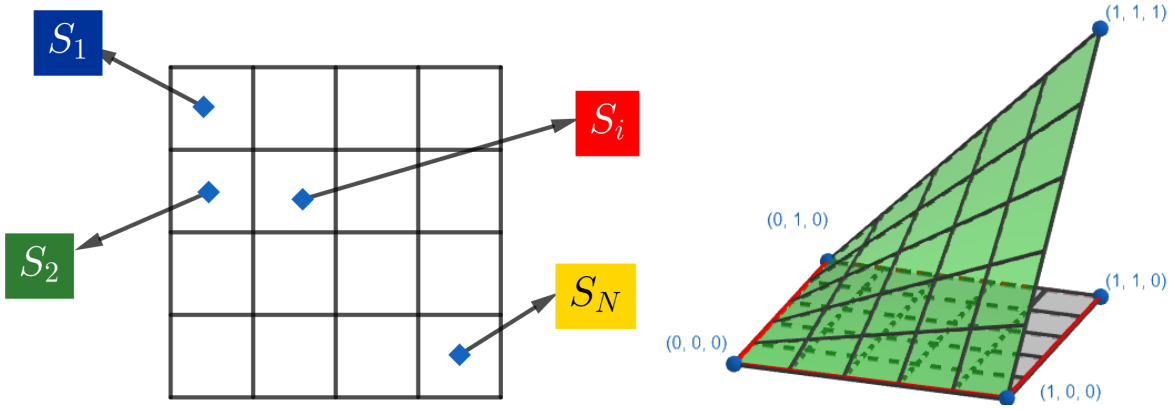

(a) Mesh and elements (b) Basis function in an element

Figure 2: Proposed element space

The Petrov-Garlekin formulation of (2) is find $u_0, ..., u_M \in Q_1$ such that

$$\begin{gathered} \iint_\Omega u_n v \, dA + \Delta t_n \iint_\Omega k \nabla u_n \cdot \nabla v \, dA = \iint_\Omega u_{n-1} v \, dA \\ u_0 = \hat{I}(x,y), \quad \textit{for each } v \in Q_1 \textit{ and } n = 1, 2, \ldots, M \end{gathered} \tag{3}$$

where $\hat{I}(x,y)$ is the projection of $I(x,y)$ onto Q_1.

Existence of the solution

To prove the existence of the solution is sufficent to prove that there is a sequence of functions u_n satisfying (2)[1] for $n = 0, 1, \ldots, M$. This results in the following proposition

Proposition 1. *Let $V \subseteq H^1(\Omega)$. There is a unique sequence of functions $u_n \in V \subseteq H^1(\Omega)$ satisfying (2)[1] for $n = 1, \ldots, M$ when $u_0 \in V \subseteq H^1(\Omega)$.*

Proof. The proof is by induction on n. The idea is show from the variational problem the bilinear and the functional forms satisfy the Lax-Milgram theorem hypothesis.

[1] Changing "...for each $v \in H^1(\Omega)$..." for "...for each $v \in V \subseteq H^1(\Omega)$..."

- Base case: $n = 1$ it is observed from equation (2) the bilinear $a(u, v)$ and the functional $l(v)$ forms are

$$a(u,v) = \iint_\Omega uv \; dA + \Delta t_1 \iint_\Omega k\nabla u \cdot \nabla v \; dA, \quad l(v) = \iint_\Omega u_0 v \; dA.$$

Let $K = \Delta t_1 \max\limits_{(x,y)\in\Omega} |k(x,y)|$, $(u,v) = \iint_\Omega uv \; dA + \iint_\Omega \nabla u \cdot \nabla v \; dA$, the inner product in $H^1(\Omega)$ and $||u|| = \sqrt{(u,u)}$. By the triangle and Cauchy-Schwartz inequalities

$$\begin{aligned}
|a(u,v)| &\leq \iint_\Omega |u_1 v| \; dA + \Delta t_1 \iint_\Omega |k\nabla u_1 \cdot \nabla v| \; dA \\
&\leq \iint_\Omega |u_1 v| \; dA + K \iint_\Omega |\nabla u_1 \cdot \nabla v| \; dA \\
&\leq \iint_\Omega |u_1 v| \; dA + K \iint_\Omega |\nabla u_1 \cdot \nabla v| \; dA + \max\{0, K-1\} \iint_\Omega |u_1 v| \; dA \\
&+ \max\{0, 1-K\} \iint_\Omega |\nabla u_1 \cdot \nabla v| \; dA \\
&\leq \max\{K,1\} \Big(\iint_\Omega |u_1 v| \; dA + \iint_\Omega |\nabla u_1 \cdot \nabla v| \; dA \Big) = \max\{K,1\}(|u|,|v|) \\
&\leq \max\{K,1\} ||u|| \cdot ||v||.
\end{aligned}$$

This shows that $a(u, v)$ is continuous, using a similar argument the ellipticity of $a(u, v)$ can be proved, i.e., there is a constant $C > 0$ such that $|a(u, u)| \geq C||u||^2$. Also functional $l(v)$ is continuous since

$$\begin{aligned}
|l(v)| &\leq \iint_\Omega |u_0 v| \; dA \\
&\leq \iint_\Omega |u_0 v| \; dA + \iint_\Omega |\nabla u_1 \cdot \nabla v| \; dA \\
&\leq ||u_0|| \cdot ||v||.
\end{aligned}$$

By the the Lax-Milgram theorem there is an unique $u_1 \in V$ such that

$$a(u_1, v) = l(v), \quad \textit{for each } v \in V$$

- Inductive step: $n = l + 1$, by the induction hypothesis $u_l \in V$, the bilinear $a(u, v)$ and the functional $l(v)$ forms are

$$a(u,v) = \iint_\Omega uv \; dA + \Delta t_l \iint_\Omega k\nabla u \cdot \nabla v \; dA, \quad l(v) = \iint_\Omega u_l v \; dA.$$

Using the same proof in the case $n = 1$ the bilinear and the functional forms are continuous and the bilinear form is elliptic. By the the Lax-Milgram theorem there is an unique $u_{l+1} \in V$ such that

$$a(u_{l+1}, v) = l(v), \quad \textit{for each } v \in V.$$

By the principle of mathematical induction the proposition holds for $n = 1, 2, \ldots, N$. □

An error estimative

The P_1 linear picewise polynomials set is defined as

$$P_1 = \{E(x,y) \in H^1(\Omega) : E(x,y)|_S = a + bx + cy,\ a,b,c \in \mathbb{R},\ \textit{for each element } S \subseteq \Omega\}$$

then $P_1 \subsetneq Q_1$. An estimation error depends on the second derivative of u_n. It would be good to find a better boundary for the error in Q_1. To give an error estimate the following definitions are introduced:

- The analysis is done in each element, let S an arbitrary element, and $A_i = (a_i^1, a_i^2)$ for $i = 1, \ldots, 4$ its nodes,
- as the elements are congruent squares, let h be the length of one of the sides of one of the elements,
- let $\zeta_1(x,y),\ \zeta_2(x,y),\ \zeta_3(x,y),\ \zeta_4(x,y)$ the four basis functions defined on the element S such that, each of them are is one in one node of S and zero in the others and
- for a function v, let $\hat{I}v$ the interpolation or projection of the v onto Q_1, hence $\hat{I}v = \sum_{i=1}^{4} v(A_i)\zeta_i(x,y)$.

According the Taylor theorem for a function u_n with n fixed and each node a_i

$$u(a_i) = u(x,y) + \frac{\partial u_n}{\partial x}(x,y)\cdot(a_i^1 - x) + \frac{\partial u_n}{\partial y}(x,y)\cdot(a_i^2 - y) + \frac{\partial^2 u_n}{\partial xy}(\xi_i)\cdot(a_i^1 - x)(a_i^2 - y) + \frac{1}{2}\Big[\frac{\partial^2 u_n}{\partial x^2}(\xi_i)\cdot(a_i^1 - x)^2 + \frac{\partial^2 u_n}{\partial y^2}(\xi_i)\cdot(a_i^2 - x)^2\Big],$$

for certain ξ_i between A_i and (x,y). Let:

- $D_i(x,y) = \frac{\partial u_n}{\partial x}(x,y)\cdot(a_i^1 - x) + \frac{\partial u_n}{\partial y}(x,y)\cdot(a_i^2 - y) + \frac{\partial^2 u_n}{\partial xy}(\xi_i)\cdot(a_i^1 - x)(a_i^2 - y)$
- $L_i(x,y) = \frac{1}{2}\Big[\frac{\partial^2 u_n}{\partial x^2}(\xi_i)\cdot(a_i^1 - x)^2 + \frac{\partial^2 u_n}{\partial y^2}(\xi_i)\cdot(a_i^2 - x)^2\Big],$

then

$$\hat{I}u = u_n(x,y)\sum_{i=1}^{4}\zeta_i(x,y) + \sum_{i=1}^{4} D_i(x,y)\zeta_i(x,y) + \sum_{i=1}^{4} L_i(x,y)\zeta_i(x,y). \tag{4}$$

Proposition 2. *Let u_n with n fixed and ζ_i, D_i as said before. If for each point (x,y) there is a point $\xi_{(x,y)} \in S$ or simply ξ such that $\frac{\partial^2 u_n}{\partial xy}(\xi) = \frac{\partial^2 u_n}{\partial xy}(\xi_i)$, $i = 1, \ldots, 4$ [2], then,*

[2]This hypothesis was added to solve a technical problem in the demonstration: the dependence of ζ from A_i

- $\sum_{i=1}^{4} \zeta_i(x,y) = 1$
- $\sum_{i=1}^{4} D_i(x,y)\zeta_i(x,y) = 0.$

Proof. For the first statement a function who has a form $v(x,y) = a + bx + cy + dxy$ and is one in each node is the function $v \equiv 1$, by the uniqueness of the v in Q_1 the first statement is concluded.

Let $v(x,y) = bx + cy + dxy$, with $b, c, d \in \mathbb{R}$ since $v \in Q_1$ then $v = \hat{I}v$. Using

$$v = \hat{I}v = v(x,y) + \sum_{i=1}^{4} \Big[(b+dy)(a_i^1 - x) + (c+dx)(a_i^2 - y) + d(a_i^1 - x)(a_i^2 - y)\Big]\zeta_i(x,y),$$

hence

$$0 = \sum_{i=1}^{4} \Big[(b+dy)(a_i^1 - x) + (c+dx)(a_i^2 - y) + d(a_i^1 - x)(a_i^2 - y)\Big]\zeta_i(x,y), \tag{5}$$

how this is valid for all values b, c, d, observing (5), take the following choices separately

- $b = \dfrac{\partial u_n}{\partial x}(x,y),\ c = \dfrac{\partial u_n}{\partial y}(x,y),\ d = 0$, to get

$$0 = \sum_{i=1}^{4} \Big[\frac{\partial u_n}{\partial x}(x,y) \cdot (a_i^1 - x) + \frac{\partial u_n}{\partial y}(x,y) \cdot (a_i^2 - y)\Big]\zeta_i(x,y), \tag{6}$$

- $b = 1,\ c = d = 0$, implies that

$$0 = \sum_{i=1}^{4} (a_i^1 - x)\zeta_i(x,y), \tag{7}$$

- $c = 1,\ d = d = 0$, implies that

$$0 = \sum_{i=1}^{4} (a_i^2 - y)\zeta_i(x,y), \tag{8}$$

multiplying (7) and (8) by $\beta + \delta y$ and $\gamma + \delta x$ respectively

$$\begin{aligned} 0 &= \sum_{i=1}^{4} (\beta + \delta y)(a_i^1 - x)\zeta_i(x,y) \\ 0 &= \sum_{i=1}^{4} (\gamma + \delta x)(a_i^2 - y)\zeta_i(x,y), \end{aligned} \tag{9}$$

with $\beta, \gamma, \delta \in \mathbb{R}$. This leads to

$$0 = \sum_{i=1}^{4} \Big[(\beta + \delta y)(a_i^1 - x)\zeta_i(x,y) + (\gamma + \delta x)(a_i^2 - y)\Big]\zeta_i(x,y), \tag{10}$$

observing the equations (5), (10) and taking $\beta = b,\ \gamma = c,\ \delta = d$ is shown that

$$0 = \sum_{i=1}^{4} \Big[(b + dy)(a_i^1 - x) + (c + dx)(a_i^2 - y)\Big]\zeta_i(x,y), \tag{11}$$

replacing (11) in (5) leads to

$$0 = \sum_{i=1}^{4} d(a_i^1 - x)(a_i^2 - y)\zeta_i(x,y), \tag{12}$$

for $d \in \mathbb{R}$.

On other hand, take $d = \dfrac{\partial^2 u_n}{\partial xy}(\xi) = \dfrac{\partial^2 u_n}{\partial xy}(\xi_i)$ (using the additional hypothesis), to get

$$\begin{aligned} 0 &= \sum_{i=1}^{4} \frac{\partial^2 u_n}{\partial xy}(\xi)(a_i^1 - x)(a_i^2 - y)\zeta_i(x,y) \\ &= \sum_{i=1}^{4} \frac{\partial^2 u_n}{\partial xy}(\xi_i)(a_i^1 - x)(a_i^2 - y)\zeta_i(x,y), \end{aligned} \tag{13}$$

combining (6) and (13)

$$\begin{aligned} 0 &= \sum_{i=1}^{4} \Big[\frac{\partial u_n}{\partial x}(x,y)\cdot(a_i^1 - x) + \frac{\partial u_n}{\partial y}(x,y)\cdot(a_i^2 - y)\Big]\zeta_i(x,y) + \sum_{i=1}^{4} \frac{\partial^2 u_n}{\partial xy}(\xi)(a_i^1 - x)(a_i^2 - y)\zeta_i(x,y) \\ &= \sum_{i=1}^{4} \Big[\frac{\partial u_n}{\partial x}(x,y)\cdot(a_i^1 - x) + \frac{\partial u_n}{\partial y}(x,y)\cdot(a_i^2 - y) + \frac{\partial^2 u_n}{\partial xy}(\xi)(a_i^1 - x)(a_i^2 - y)\Big]\zeta_i(x,y) \\ &= \sum_{i=1}^{4} D_i(x,y)\zeta_i(x,y), \end{aligned}$$

the desired result is obtained. □

Finally, Cea's lemma is used, let $\{u_n\}_{n=0,\dots,M}$ the sequence of functions satisfying (2), and $\hat{u_n}$ the sequence of functions satisfying (3), those functions exist by the proposition 2, Cea's lemma guarantees that exists a constant $C > 0$ such that

$$||u_n - \hat{u_n}||_{L_\infty(S)} \leq C||u_n - v||_{L_\infty(S)},\ \textit{for each } v \in Q_1 \textit{ and each } n. \tag{14}$$

Taking $v = \hat{I}u_n$, and the proposition 2

$$\hat{I}u_n - u_n = \sum_{i=1}^{4} L_i(x,y)\zeta_i(x,y),$$

then,

$$\begin{aligned} |\hat{I}u_n - u_n| &\leq \Big| \sum_{i=1}^{4} L_i(x,y)\zeta_i(x,y) \Big| \\ &\leq \sum_{i=1}^{4} |L_i(x,y)\zeta_i(x,y)|, \end{aligned}$$

note that $\zeta_i(x,y) \geq 0$ for $i = 1, \ldots, 4$. Hence

$$\begin{aligned} \sum_{i=1}^{4} |L_i(x,y)\zeta_i(x,y)| &\leq \sum_{i=1}^{4} \max_{(x,y)\in S} |L_i(x,y)|\zeta_i(x,y) \\ &\leq \sum_{\substack{i=1 \\ i=1,\ldots,4}}^{4} \max_{(x,y)\in S} |L_i(x,y)|\zeta_i(x,y) \\ &= \max_{\substack{(x,y)\in S \\ i=1,\ldots,4}} |L_i(x,y)| \sum_{i=1}^{4} \zeta_i(x,y) \\ &= \max_{\substack{(x,y)\in S \\ i=1,\ldots,4}} |L_i(x,y)|. \end{aligned} \tag{15}$$

On other hand, for each i

$$\begin{aligned} |L_i(x,y)| &= \Big| \frac{1}{2} \Big[\frac{\partial^2 u_n}{\partial x^2}(\xi) \cdot (a_i^1 - x)^2 + \frac{\partial^2 u_n}{\partial y^2}(\xi) \cdot (a_i^2 - y)^2 \Big] \Big| \\ &\leq \frac{h^2}{2} \Big(\Big| \frac{\partial^2 u_n}{\partial x^2}(\xi) \Big| + \Big| \frac{\partial^2 u_n}{\partial y^2}(\xi) \Big| \Big), \end{aligned} \tag{16}$$

using (15) and (16)

$$\begin{aligned} ||\hat{I}u_n - u_n||_{L_\infty(S)} = \max_{(x,y)\in S} |\hat{I}u_n - u_n| &\leq \max_{(x,y)\in S} \Big\{ \frac{h^2}{2} \Big(\Big| \frac{\partial^2 u_n}{\partial x^2}(x,y) \Big| + \Big| \frac{\partial^2 u_n}{\partial y^2}(x,y) \Big| \Big) \Big\} \\ &= \frac{h^2}{2} \max_{(x,y)\in S} \Big\{ \Big| \frac{\partial^2 u_n}{\partial x^2}(x,y) \Big| + \Big| \frac{\partial^2 u_n}{\partial y^2}(x,y) \Big| \Big\}, \end{aligned} \tag{17}$$

applying Cea's lemma (14) to (17)

$$||\hat{I}u_n - u_n||_{L_\infty(S)} \leq C \frac{h^2}{2} \max_{(x,y)\in S} \Big\{ \Big| \frac{\partial^2 u_n}{\partial x^2}(x,y) \Big| + \Big| \frac{\partial^2 u_n}{\partial y^2}(x,y) \Big| \Big\}. \tag{18}$$

This results in an estimate of the error in the norm $L_\infty(S)$. This error is a bit better compared to the error for the space P_1:

$$||\tilde{I}u_n - u_n||_{L_\infty(S)} \leq 2Ch^2 \max_{|\alpha|=2} \left\{ \left|\left| \frac{\partial^\alpha u_n}{\partial x^\alpha}(x,y) \right|\right|_{L_\infty(S)} \right\} \tag{19}$$

where $\tilde{I}v$ is the interpolation on P_1 of the function v and α is multi-index indicating all derivatives with order α.

Assembling matrices

From (3) two matrices and a vector must be assembled, the solution u is defined as

$$u(x,y,t) = \sum_{i=1}^{N} \alpha_i(t)\phi_i(x,y),$$

where $\phi_i(x,y)$ is a basis function defined on Ω, $\alpha_i(t)$ is a coefficient that depends of the time and N is the number of basis functions. By the definition of u_n, $u_n(x.y) = \sum_{i=1}^{N} \alpha_i(t_n)\phi_i(x,y)$. Let $\alpha_n = (\alpha_1(t_n), \ldots, \alpha_N(t_n))^t$, when the equation (3) is observed, the vector v can be changed by $v = \phi_i(x,y)$, that is, only using the basis functions. Thus the formulation changes to: find a sequence of vectors $\alpha_0, \ldots, \alpha_n$, such that

$$\begin{gathered} \sum_{i=1}^{n} \alpha_i(t_n) \iint_\Omega \phi_i\phi_j \, dA + \Delta t_n \sum_{i=1}^{n} \alpha_i(t_n) \iint_\Omega k\nabla\phi_i \cdot \nabla\phi_j \, dA = \sum_{i=1}^{n} \alpha_i(t_{n-1}) \iint_\Omega \phi_i\phi_j \, dA \\ \alpha_0 = (I(x_1,y_1), \ldots, I(x_N,y_N))^t, \quad for\ i,j = 1,2,\ldots,M \ and\ n = 1,2,\ldots,M, \end{gathered} \tag{20}$$

where $\{(x_k,y_k)\}_{k=1,\ldots,N}$ go through all the nodes. The mass matrix $\mathcal{M}$ and stiffness matrix $\mathcal{S}$ are defined as

$$\mathcal{M}ij = \iint_\Omega \phi_i\phi_j \, dA, \ and\ \mathcal{S}_{ij} = \iint_\Omega k\nabla\phi_i \cdot \nabla\phi_j \, dA, \ for\ i,j = 1,\ldots,N, \tag{21}$$

using this the formulation (20) can be rewritten as a matrix-vector product

$$\begin{gathered} (\mathcal{M} + \Delta t_n \mathcal{S})\alpha_n = M\alpha_{n-1} \\ \alpha_0 = (I(x_1,y_1), \ldots, I(x_N,y_N))^t. \end{gathered}$$

To calculate the integrals mentioned in (21) a extension of a three point Gauss quadrature rule is used, this rule uses 9 points in each element, that is, for a function f defined in Ω

$$\iint_\Omega f(x,y) \, dA \approx \sum_{i=1}^{9} w_i f(x_i,y_i) \tag{22}$$

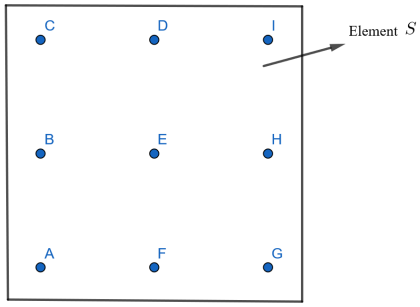

Figure 3: Quadrature rule referring to (22)

this allows calculating those integrals quickly. Also, mass and stiffness matrices are both positive defined, algorithms like Cholesky's factorization, ldl or conjugate gradient can be used to perform the equation resolution.

Results

In the following, several results with different diffusion coefficients are shown. Depending on this we have different results

- Constant diffusion coefficient: $k = 1$, simulates an unfocused image, the image has dimensions 400×400 pixels and $T = 5$.

(a) Real image (b) Blurred image

Figure 4: Case 1, crying goddess blur. Recovered from [8]

- Constant diffusion coefficient: $k = 1$, simulates an unfocused image, the image has dimensions 499×459 pixels and $T = 15$.

(a) Real image (b) Blurred image

Figure 5: Case 2, diagonal argument blur. Recovered from [5]

- Constant diffusion coefficient: $k = 2$, simulates an unfocused image, the image has dimensions 495×369 pixels and $T = 10$.

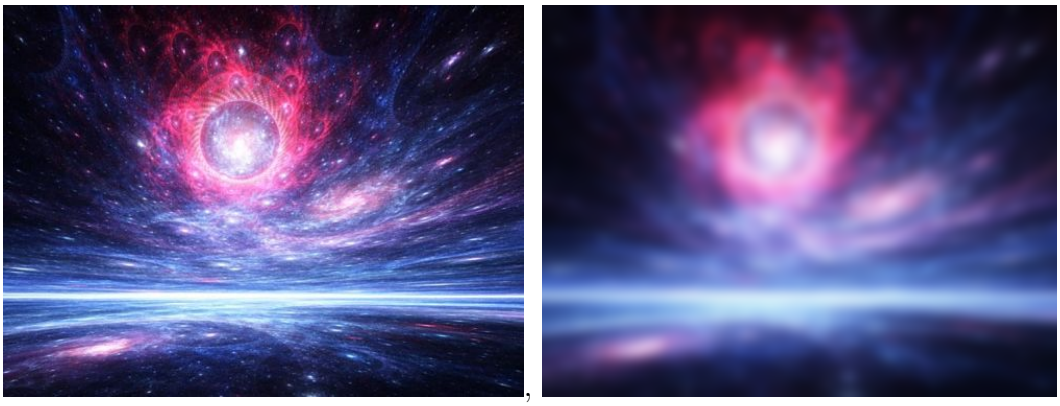

(a) Real image (b) Blurred image

Figure 6: Case 3, image galaxy blur. Recovered from [3]

- Variable diffusion coefficient: $k(x, y) = f(r)$, where $f(r)$ is a function that depends on the distance r from the point (x, y) at the center of the image, this simulates the blurring of the background when a camera takes a picture, where

$$f(r) = \left(\frac{r}{\eta}\right)^3 \quad and \quad \eta = \frac{1}{2}\max(a, b)$$

with a, b the dimensions of the image. The image has dimensions 498×391 pixels and $T = 5$.

(a) Real image (b) Blurred image

Figure 7: Case 4, dandelion camera focus. Recovered from [4]

- Coefficient of constant matrix diffusion: $k \in \mathcal{M}_{2\times 2}(\mathbb{R})$. In this case

$$k = \frac{1}{8}\begin{bmatrix} 65 & -63 \\ -63 & 65 \end{bmatrix}$$

and simulates the blurring effect of an object in motion. In this case the dithering has preferential directions: the eigenvectors of k. The image has dimensions 700×525 pixels and $T = 20$.

(a) Real image (b) Blurred image

Figure 8: Case 5, license plate motion blur. Recovered from [10]

Conclusions and discussion

Blurred images appear in several problems and applications in images, a model of blurred images using PDE's is shown. The hypothesis of the boundary conditions, source term, nodes, elements, and basis functions appear naturally from the blur hypothesis in the image problem or application. The shown results become realistically to reproduce diverse situations of degraded images.

The number of elements is $(a-1)(b-1)$ when the image has dimensions $a \times b$ pixels, in this context appear large and sparse systems of equations. M systems of equations must be solved to obtain the solution; the advantage is that in principle the diffusion coefficient k doesn't depend on the time, this implies the mass and stiffness matrices are assembled once. A problem is to assemble these matrices quickly.

In this work is the open question that investigates whether it is possible to weaken or remove the hypothesis added in proposition 2.

Future work will find a faster algorithm to assemble the mass and stiffness matrices, on the other hand, develop an algorithm to deblur images using this work as a subroutine of the deblurring process.

References

[1] Jochen Alberty, Carsten Carstensen, and Stefan A Funken. Remarks around 50 lines of matlab: short finite element implementation. *Numerical Algorithms*, 20(2-3):117–137, 1999.

[2] William E Boyce, Richard C DiPrima, and Douglas B Meade. *Elementary differential equations*. John Wiley & Sons, 2017.

[3] [Gráficos de galaxia] . (n.d.). Retrieved July 21 2019. https://www.freepik.es/fotos-vectores-gratis/galaxia.

[4] [Diente de León]. (n.d.). Retrieved July 21 2019. http://hablemosdeflores.com/diente-de-leon/.

[5] [Argumento diagonal]. (n.d.). Retrieved July 21 2019. https://es.wikipedia.org/wiki/argumentodeladiagonaldecantor.

[6] Claes Johnson. *Numerical solution of partial differential equations by the finite element method*. Courier Corporation, 2012.

[7] Sirisha L Kala. Deblurring images via partial differential equations. *Proceedings of the Louisiana-Mississippi Section of the Mathematical Association of America*, 2004.

[8] [Godness Aqua]. (n.d.). Retrieved July 21 2019. https://www.redbubble.com/3790348-chibi-llorando-aqua?p=sticker/.

[9] [Northern Lights]. (n.d.). Retrieved July 21 2019. http://misistemasolar.com/aurora-boreal/.

[10] [Car plate]. (n.d.). Retrieved July 21 2019. from https://www.flickr.com/photos/pattoncito/2471478157.

[11] Charles F Van Loan and Gene H Golub. *Matrix computations*. Johns Hopkins University Press Baltimore, 1983.